We are IntechOpen, the world's leading publisher of Open Access books Built by scientists, for scientists

6,900
Open access books available

186,000
International authors and editors

200M
Downloads

Our authors are among the

154
Countries delivered to

TOP 1%
most cited scientists

12.2%
Contributors from top 500 universities

WEB OF SCIENCE™

Selection of our books indexed in the Book Citation Index
in Web of Science™ Core Collection (BKCI)

Interested in publishing with us?
Contact book.department@intechopen.com

Long Wavelength VCSELs and VCSEL-Based Processing of Microwave Signals

M. E. Belkin, L. Belkin, A. Loparev, A. S. Sigov and
V. Iakovlev

Additional information is available at the end of the chapter

Abstract

We address the challenge of decreasing the size, cost and power consumption for practical applications of next generation microwave photonics systems by using long-wavelength vertical cavity surface emitting lasers. Several demonstrations of new concepts of microwave photonics devices are presented and discussed.

Keywords: Vertical cavity surface emitting laser, microwave photonics, optoelectronic processing

1. Introduction

Microwave photonics (MWP) is a relatively new branch of science and technology gradually penetrating into telecom (ultra-high-speed optical fiber systems, fiber-to-wireless (FiWi) access networks) and defense (phased-array antenna radars, electronic warfare (EW) systems) industries. Progress in developing MWP solutions is mainly following the progress in low cost and high power, efficient optical sources [1]. Among other semiconductor laser technologies, long-wavelength vertical cavity surface emitting lasers (LW-VCSELs) are regarded as an enabler for superior features in high-performance photonic circuits [2], and have the potential to do so for MWP as well [3]. In fact, the application of LW-VCSELs emitting in the telecom wavelength range is expected to benefit from the availability of low cost components already developed in the framework of information and communication technology (ICT) [2]. However, as compared with other applications of VCSELs (datacom, sensing, etc.), their use in

MWP requires paying further attention to their spectral purity, noise, single-mode operation, and linearity features [4]. Specifically, the possibility of wavelength division multiplexing (WDM) and the low sensitivity to electromagnetic perturbations of optical fiber-based transmission allow the introduction of novel concepts into on-board or ground-based modules for antenna's remote control, signal distribution and processing of broad-bandwidth analogue signals. For example, the development of electrical-to-optical converters is in fact a continuous challenge for lower noise and higher linearity, which would be fully compatible with the required dynamics in phased-array antennas. Therefore, for the next generations of telecom and radar microwave-to-fiber systems, it is imperative to find solutions for increasing the spurious-free dynamic range (SFDR) of photonic devices and links. In addition, the penetration of optoelectronic technologies into modern radar systems has also been realized through the optical implementation of a large number of vital functions like optical beam-forming, adaptive filtering or microwave signal analog-to-digital conversion [5, 6].

In view of these trends, the engineering and cost benefits of VCSELs make them increasingly attractive for optical fiber–based applications [7] in general and for microwave photonics in particular. That is why there is an increasing interest to evaluate the potential of LW-VCSELs for microwave photonics application areas [4].

Starting from 1990s, the development of LW-VCSEL technology was benefitting from what is known today as the 'telecom bubble', with the main motivation coming from high-bandwidth (mainly metropolitan) optical networks.

It was expected that LW-VCSEL technology will follow the success story of short-wavelength spectral range ($\lambda \sim 800$–1000 nm) VCSEL technology. It turns out that the main difficulty of LW-VCSELs technology is the need of having in a monolithic semiconductor device the active materials providing high optical gain and mirrors with high-reflectivity, low optical absorption and high thermal conductivity. The best semiconductor materials for these tasks are, from one side, InP/InAlGaAs quantum wells (InP based) and, from another side, GaAs/AlGaAs DBRs (GaAs based). Unfortunately, these semiconductor structures are mutually incompatible from the epitaxial growth point of view, even virtually impossible to grow such VCSELs structure in all-epitaxial growth fabrication approach. This difficulty has triggered many attempts to develop LW-VCSELs to overcome this materials problem without yielding the expected results. As a result, the progress in development of long-wavelength VCSEL technology was much slower than initially expected.

As of today, we see progress in LW-VCSELs development and industrialization towards meeting the requirements of previously identified applications as well as toward the new emerging application areas [8]. This progress is supported only by a few technologies, which have proven to yield LW-VCSEL with acceptable performance [2]. It turns out, that so called wafer-fused LW-VCSEL technology, that is employing strained InP/InAlGaAs quantum well active regions, tunnel junction and GaAs/AlGaAs distributed Bragg reflectors for generation of photons, carrier and optical confinement and for optical feedback respectively is the only technology that have reached the industrial production stage and proven reliability [2, 8]. A particular advantage of these industrially fabricated LW-VCSELs is in covering the full ITU-T spectral range from O-band to U-band. Concerning MWP, an important feature of LW-

VCSELs is their adaptability with future silicon-based photonic integrated circuits, which should provide many advantages when implementing microwave photonic devices and techniques. Investigations of VCSEL-based MWP devices enabled to find and exploit unique features of LW-VCSELs, for example, excellent compatibility with optical injection locking techniques to enhance key dynamic features (modulation bandwidth, extinction ratio, SFDR) [9]. A specific benefit of LW-VCSELs is the suitability for silicon large-scale integrated technology where it could effectively be used as source and modulator for optical interconnects [10].

In this chapter we will describe benefits of long wavelength wafer-fused VCSEL compared with other types of optical sources, double fused LW-VCSEL design and fabrication, procedure and results of Telcordia-grade reliability testing, metrology and characteristics of the devices, VCSEL-based devices processing of microwave signals and future trends in long wavelength VCSEL photonics.

2. Benefits of Long Wavelength Wafer-Fused VCSEL

The ongoing success of VCSELs is particularly due to the intrinsic advantages of this laser type as compared to the edge-emitting laser diodes. The most important features of VCSELs are their low beam divergence leading to relaxed fiber alignment tolerances, the small threshold currents and high slope efficiencies leading to low electrical power consumption, and their potential for integration to 1D and 2D laser arrays. Additionally, VCSELs are usually longitudinal single-mode [11].

All the short wavelength VCSEL features hold for the VCSELs operating at long wavelength range beyond 1.3 µm. In addition, for geometrical reasons, the longer wavelengths make the transverse mode and polarization control easier so that true single-mode devices with a stable polarization may be achieved even for rather large current aperture diameters of around 5–7 µm [12, 13]. Accordingly, long-wavelength VCSELs have a tremendous meaning for a wide variety of applications, ranging from short to long range optical communications, parallel data transmission as well as optical measurement and gas sensing. In many of these applications, therefore, long-wavelength VCSELs turn out to be cost-effective and superior performance substitutes for conventional Fabry-Perot or distributed feedback (DFB) lasers [2, 10]. As compared with edge emitting technology, the main advantage is the fact that devices can be fully tested on wafer, without the need to form laser resonator by cleaving. In fact VCSEL technology is similar to LED technology that is yielding light emitting devices with the quality of beam much superior as compared with the beam of edge emitting laser.

For ICT, for example, in [14] it was demonstrated an order of magnitude better efficiency for a VCSEL in comparison to that for a DFB laser for radio frequency (RF) to optical power conversion. The performance of optical link comprising wired and wireless circuits with direct modulation have confirmed the viability of VCSELs as power-efficient optical sources. According to the results of detailed investigation of VCSEL-based optoelectronic frequency converter and novel sub-harmonic frequency multiplicator for the circuitry of RoF's systems [15], the potential of long wavelength VCSEL based MWP devices for the application in future

equipment for ultra-wide band telecom and radar systems and in measurement techniques is demonstrated.

3. Design and fabrication.

As stated above, the development of LW-VCSELs has converged to only a few technology solutions for fabrication of devices with performances matching and even surpassing state of the art short-wavelength VCSEL. Three main common elements of these few technology solutions should be outlined. First, the strained InP/InAlGaAs quantum wells for high optical gain at high temperatures. Second, GaAs/AlGaAs or dielectric distributed Bragg reflectors (DBR) for high mirror reflectivity. Third, the tunnel junctions for intra-cavity contacting to reduce mirror optical loss. In Table 1 [2] it is presented a summary of the three main approaches that are currently being used in LW-VCSEL design, as well as the resulting device performance.

Aperture type	Mirror design	SM P_{max}, 20 °C	SM P_{max}, 80 °C
Undercut QWs	Top and bottom as-grown DBRs: InAlGaAs/InAlAs, or AlGaAsSb	1.6 mW	0.5 mW @ 70
Buried TJ	One as-grown InAlGaAs /InAlAs DBR; one dielectric DBR	4.3 mW	1.4 mW
Regrown TJ	Both wafer-fused AlGaAs/GaAs DBRs	6 mW	2.5 mW
SM P_{max} 20 (80)°C, single-mode maximum power output at 20 °C (80 °C); TJ- tunnel junction; QW-quantum well			

**Table 1.** Performances of LW-VCSELs fabricated by three main approaches.

In the approach based on undercut quantum wells (QW) all laser cavity parts (DBRs and QWs) are fabricated epitaxially in InAlGaAs/InAlAs(InP) material system, and are grown in a single epitaxial run. In this material system it is possible to define device aperture by undercut selective chemical etching of a part of the QWs. The best devices fabricated following this approach have demonstrated quite low single-mode output of 0.5 mW at 70°C, that is rather low, mainly because of too poor thermal dissipation from the active region both in the lateral direction (through air gap) and in the vertical direction (through quaternary layers of DBR), as thermal conductivity of the InAlGaAs layers is much lower as compared with AlGaAs layers in GaAs based DBRs, normally used in the well-established short-wavelength VCSEL technology.

Further progress was made possible by introducing buried tunnel junction (TJ) for current and optical localization and a dielectric DBR. Even though the thermal dissipation is still inefficient in the vertical direction, it is considerably improved in the lateral direction because of the relatively good heat transfer through the regrown InP. This improvement enables the device to reach a single-mode output power of about 1.4 mW at 80 °C.

It turns out that the above mentioned two approaches do not show good performance devices in O-band (1300 nm wavelength range), especially at the shorter wavelengths of 1270 and 1290

nm, as compared with the performances in C-band (1550 nm waveband). On top of poor thermal characteristics, the optical properties of InP based DBRs for this wavelength suffer from the low refractive index-contrast of the 1310-nm wavelength DBR that needs to be set lower to exclude the edge-band absorption in InAlGaAs quarter-wavelength layers.

The best performances of long-wavelength VCSELs (single-mode output powers as high as 6 mW at room temperature and 2.5 mW at 80°C) are demonstrated with devices that have a regrown TJ aperture on the InAlGaAs/InP active cavity and AlGaAs/GaAs DBRs attached to this cavity using wafer fusion (Figure 1a). The results comes with enhanced thermal dissipation from the active region in both lateral (through InP spacers) and vertical directions (through GaAs based DBRs) as well as with high reflectivity and thermal conductivity of the AlGaAs/ GaAs DBRs. With such performances VCSELs may be used in both single- and multi-channel applications. Wafer fusion for LW-VCSEL fabrication was pioneered by the group at the University of California in Santa Barbara in 1995, but without regrown tunnel junction (current localization were performed by introducing an oxide aperture in the same way as for 850-nm wavelength VCSELs).
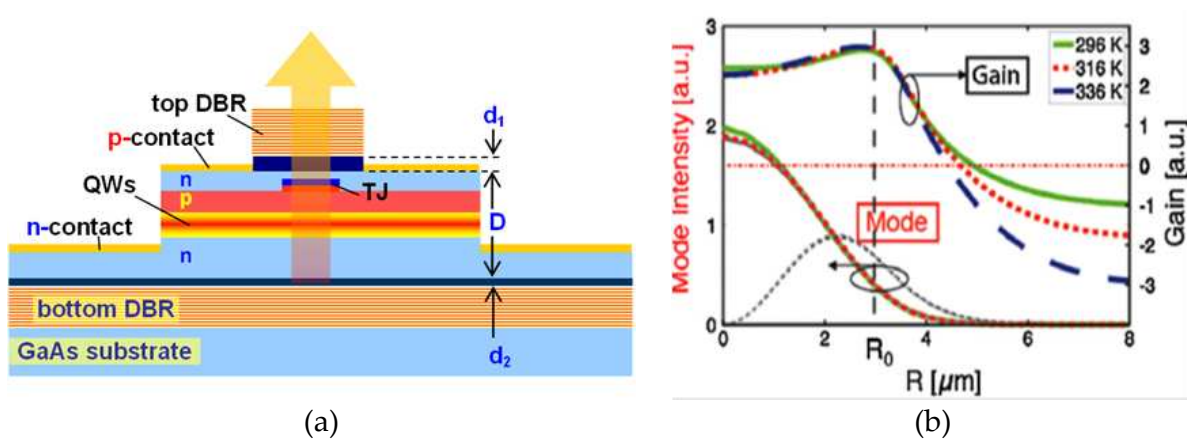

Figure 1. (a) Schematic sectional presentation of the wafer-fused VCSEL; (b) Radial gain and optical field distributions of a device with 3um TJ mesa radius (R_0)

VCSEL's wafer fabrication is schematically depicted in Figure 2. Below is the description of the details of double fused LW-VCSEL design and fabrication process as described in [8]. The VCSEL has an InP-based $5/2\lambda$-active cavity. Un-doped AlGaAs/GaAs DBRs are wafer fused on both side of this cavity, as schematically depicted in Figure 1a.

Four to six compressively strained quantum wells are inserted in this InAlGaAs/InP active region, as well as a p++/n++ InAlGaAs tunnel junction. All epitaxial material for the double fused wafers is grown by low pressure metal-organic vapor phase deposition (MOVPE) on 2-inch (100) wafers. The mesa-structures of 3-3.5 μm radius is formed in the tunnel junction layer after first growth run, and then is re-grown with n-type InP layer. This regrown structure serves for carrier and photon confinement. The top and bottom intra-cavity n-InP layers are used for electrical contacting that allows using un-doped top and bottom DBR mirrors. It is important to note the possibility to introduce InGaAsP cavity adjustment layers in the InP

based epi structure. Such layers on both sides of the active cavity help for precise adjustment of the emission wavelength. Numerical simulations of such a structure [16] indicates (Figure 1b), that in normal operation conditions in the device, operating predominately in the fundamental mode, the gain and mode profiles spread outside the active region defined by the tunnel junction mesa by about 1–1.5 μm.
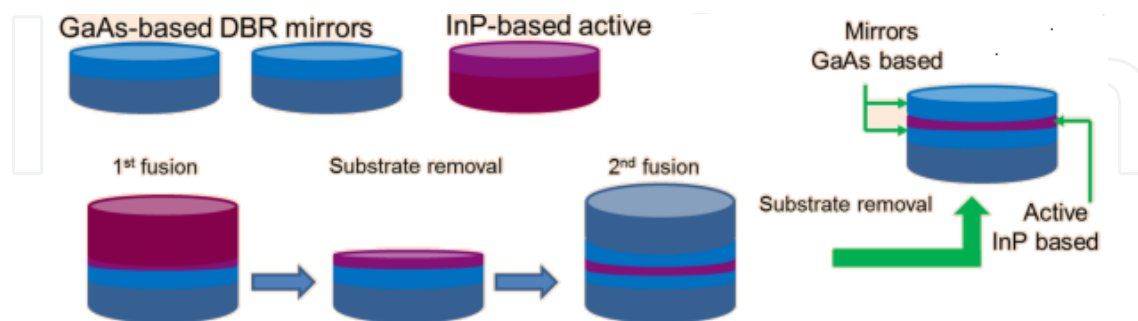

Figure 2. Fabrication of wafer-fused VCSEL

The details of fabrication process are presented in Figure 3, starting from mesas etched in the tunnel junction (a), then after re-growth (b). One can see that before first fusion step (c), and after the first fusion step (d) the surface is not flat. After re-growth the mesas have elliptical shape and a size that exceeds 2–2.5 times the initially round shaped mesas. This slight elongation of the mesas and planarization is occurring during re-growth by MOVPE. The elliptical shape of the re-grown mesa is a strong factor for discrimination of polarization modes.

The oblique line in Figure 3c depicts the border between two regions on the wafer with different cavity lengths. In wafer fusion process it is possible to have different cavity lengths on the same wafer. For this purpose, before the first fusion process, the InGaAsP cavity adjustment layer is selectively etched.

For bonding, the 2-inch wafers of InP-based active region and GaAs-based DBR are brought into contact. The parameters of the process are: vacuum better than 10^{-5} mBars, 600°C and a force of 7000 N for 30 min. The process is performed in an industrial custom-built wafer-bonding machine. At these process conditions, both wafers undergo a slight plastic deformation and a uniform contact on a nanometer scale is achieved and the strong covalent bonds are formed between atoms at interface of fused wafers. During cooling to room temperature, the wafer is bowed with a radius of curvature of about 1m due to thermal expansion coefficients mismatch between GaAs (lattice parameter of 0.5653 nm, thermal expansion coefficient 5.8×10^{-6} K^{-1}) and InP (lattice parameter of 0.5868 nm and thermal expansion coefficient 4.8×10^{-6} K^{-1}).

The selective etching the InP substrate is the releasing the strain that was bowing the fused stack, the remaining GaAs substrate with thin InP based layered active region re-gains its planarity. The second DBR is then bonded to the InP-based active cavity in the second fusion process under the same conditions as during the first fusion. After the second fusion the fused stack is no longer bowed. SEM and TEM micrographs of the double-fused VCSEL hetero-structure are depicted in Figure 4. High resolution SEM and TEM images indicate that the
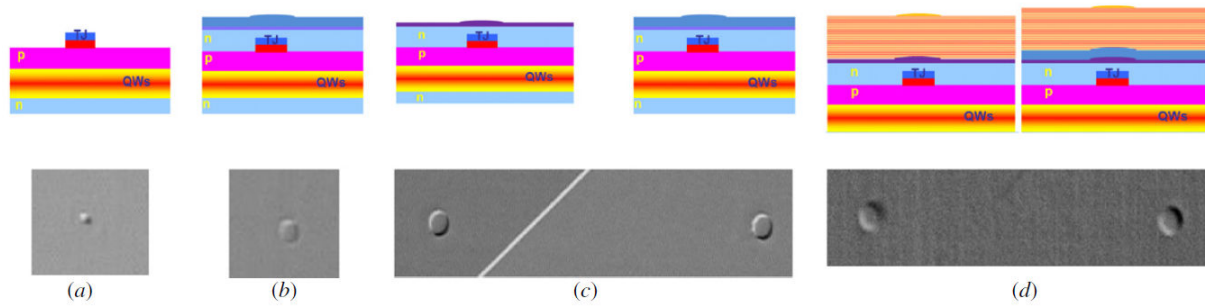
Figure 3. Images of TJ mesas: (a) initially etched 7μm mesas, (b) re-grown mesas, (c) before fusion, (d) after fusion.
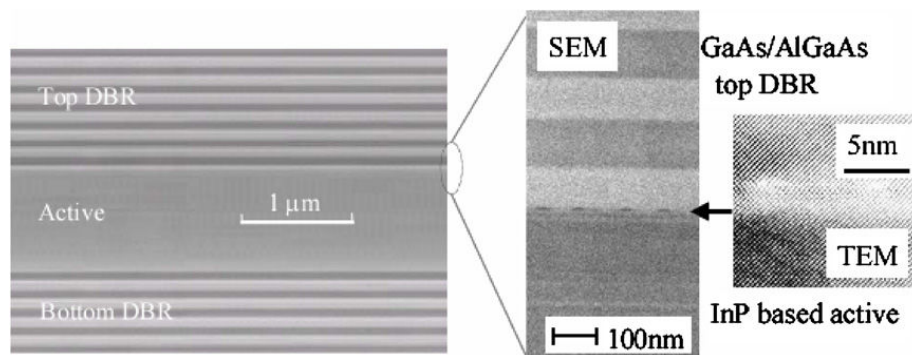
**Figure 4.** SEM and TEM micrographs of the double-fused VCSEL wafer.
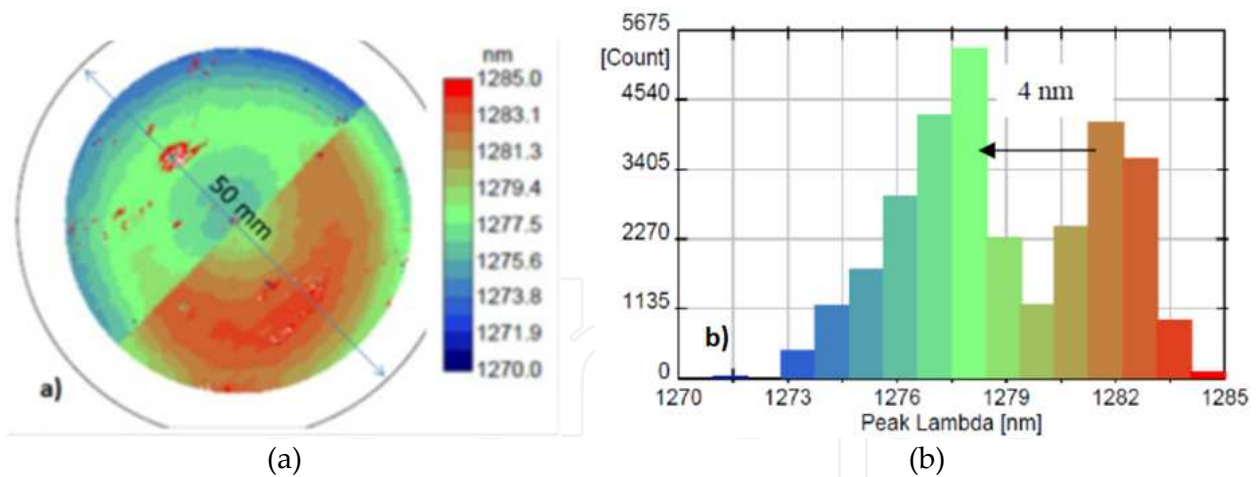
Figure 5. a) Map of a wafer. Cavity adjustment was performed on half of the wafer; b) Histograms of the cavity wavelength across the wafer shown in Figure 2. a)

misfit dislocations resulting from the lattice mismatch of GaAs and InP are well confined only at the fused interface and do not propagate inside the VCSEL structure. As presented in [17], the high quality of bonding process was attested by reliability tests of fabricated devices. Figure 5, a, depicts the cavity length distribution obtained from photoluminescence emission spectra mapping on the double-fused wafer under optical pumping with a 980-nm laser pump spot

of 5 μm diameter with 0.1 mm step. One can observe two regions with different emission wavelengths resulting from the cavity engineering performed before the first fusion, as described above. In this way one can perform wavelength control in fabrication of wafer fused VCSELs by applying a nanometer precision cavity adjustment. In more details the procedure and results of cavity length adjustment is presented in [18] and is described shortly below.

The strategy for increasing the yield of wavelength setting in wafer-fused VCSELs consists in working with batches of identical wafers (at least 3 batches, see Figure 2) of InP-based active cavity material and DBR. After fabricating the first double-fused VCSEL wafer and measuring the emission wavelength distribution, it is possible to introduce corrective actions when fabricating the next wafers for improving the emission wavelength setting yield. For the situations when the emission wavelength distribution is shifted to longer wavelengths relative to the requested wavelength slot, a nanometer precision cavity trimming technique [18] was developed. According to this technique, several oxidation-desoxidation calibrated steps (that removes one nanometer at one step) were performed in order to decrease the effective cavity length. Figure 5a depicts the cavity mode wavelength mapping of a VCSEL wafer on which half wafer has undergone 4 of such cavity etching steps before fusing to the bottom DBR. As one can see from Figure 5b, the distribution peak of cavity wavelength on the adjusted part of the wafer is shifted by 4 nm relative to the cavity distribution on the non-etched part.
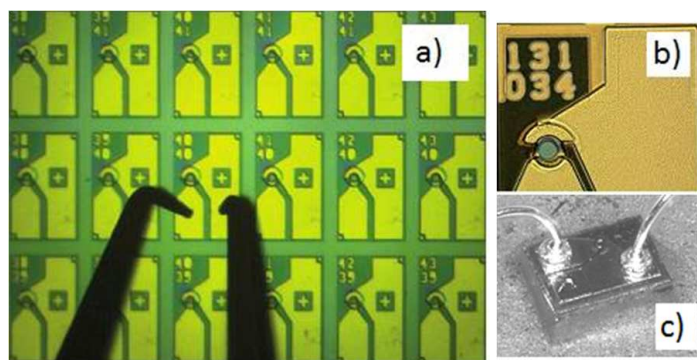

Figure 6. a) Microscope picture of the VCSEL wafer under test, b) VCSEL chip with electroplated contact pads, c) 250x350μm VCSEL chip mounted on header.

The processing of the double-fused VCSEL wafer includes (i) reactive ion etching of the top DBR, (ii) selective chemical etching steps in the InAlGaAs/InP active cavity region, (iii) dielectric deposition, (iv) dry etching steps and (v) e-beam deposition of metals for contacts. The processed VCSEL wafer (Figure 6) offers on-wafer testing possibility that decrease manufacturing cost as compared to edge emitting lasers. Full wafer electroplating for bond pads allows depositing thick metal that is a benefit for wire bonding.

The industrialization of above presented VCSEL technology was started for wavelength division multiplied (WDM) optical fiber communication applications. In ref. [19], it was demonstrated that devices with single-mode emission power in excess of 1.2mW in the temperature range of 20-80°C at operating voltage below 2.5 V, single-mode emission with 40-

dB side mode suppression ratio are in compliance with the requirements of the 10 GBASE-LX4 IEEE.802.3ae standards. The progress in 1300 nm wavelength wafer-fused VCSELs was backed by the progress in 1500 nm wafer-fused VCSELs [20]. The recent status of wafer-fusion VCSEL technology [21], as compared with its status presented earlier [2], is a result of the dramatic improvement of the quality of the final double fused-wafer as well as of the processing steps that allows a successful demonstration of their reliability.

In Figure 7 [22] are presented examples of the VCSEL chip SEM cross section overview (a) and high resolution SEM of TJ region.
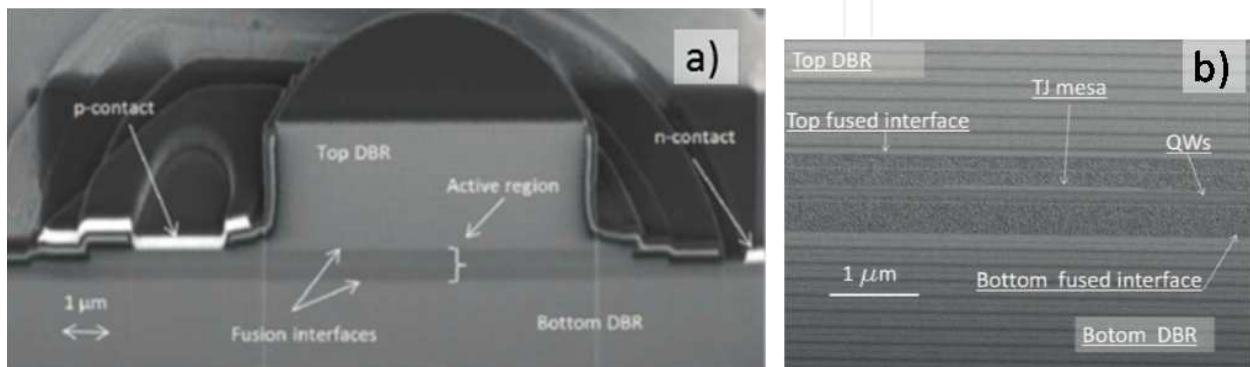

Figure 7. SEM of VCSEL chip cross section overview (a) and high resolution SEM of TJ region (b)

4. Telcordia-grade reliability testing

For the reliability tests, VCSELs were assembled onto hermetically sealed standard headers. A burn-in (BI) procedure has been designed and applied in order to exclude any early period failure. Reliability tests were performed according to the GR-468-CORE Telcordia Generic Reliability Assurance Requirements for Optoelectronic Devices [23]. Overall, the tests have demonstrated that wafer-fused VCSELs behave like any other all-grown laser devices. The emission power in time of a qualification lot of 11 devices at 10 mA and ambient temperature of 90°C that correspond to a junction temperature close to 120°C and to a current density through the tunnel junction of 26 kA/cm² is depicted in Figure 8. One cannot see any visible degradation at these operating conditions during 5000 hours of operation. Four more groups of devices from the same VCSEL wafer were tested for accelerated wear-out at higher values of junction temperature and current densities, as shown in Figure 8. The performance of devices was periodically tested at room temperature. Figure 9 depicts evolution in time of emission power at 9 mA (left graph) and threshold current (right graph) of a group of 8 devices under aging test at 10 mA and temperature 150°C. Under these test conditions one can observe devices with small changes (for example, devices 32, 35, 37) in output power and threshold current and devices that show more pronounced gradual degradation, like devices 30, 31, 33 and 36. Based on the statistical distributions of the totality of accelerated lifetime test (ALT) data, VCSEL aging parameters were calculated: activation energy value of E_a=0.67 eV and

current exponent factor N=3.93. The value of activation energy of 0.67 eV is close to 0.79 eV - the activation energy of 1550 nm VCSELs with active region in the same (InAlGaAs/InP) material system grown by MOVPE [24], even though devices with undercut apertures investigated in [24] do not exhibit gradual wear-out in time during ALT tests. Predicted operation lifetimes are calculated based on the accelerated life-time data and applying the acceleration factors and the pass-fail condition of 2-dB change. The maximum driving current for VCSELs is set 9 mA which is quite sufficient for high-speed modulation at 8-9 mA bias current and the maximum ambient operating temperature is set to 70°C according to telecom industry requirements.
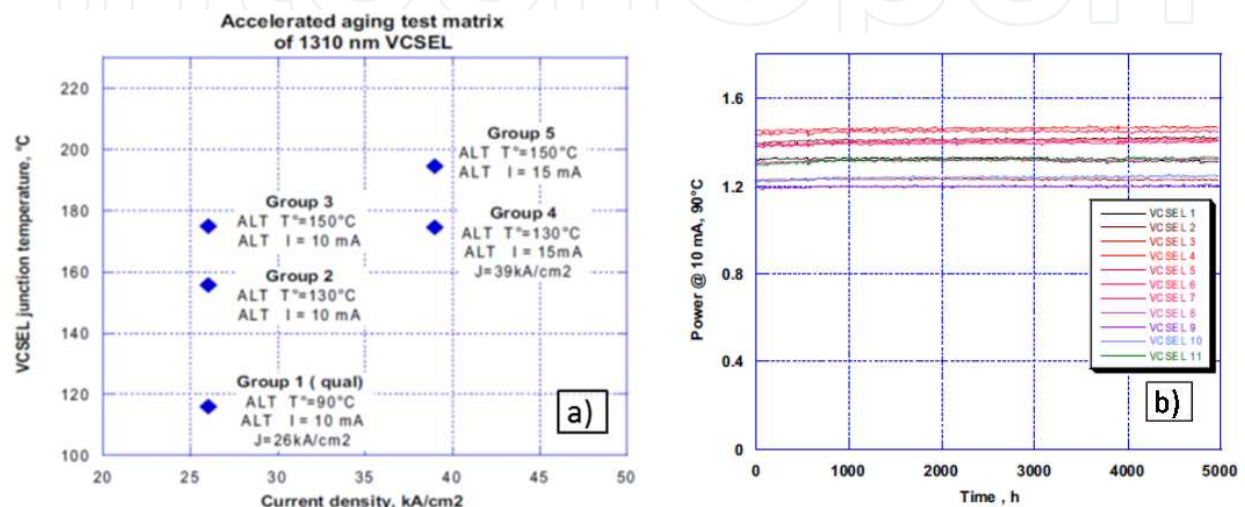

Figure 8. a) Accelerated aging test matrix and b) Emission power in time of 11 devices operating at 10 mA driving current and ambient temperature of 90°C
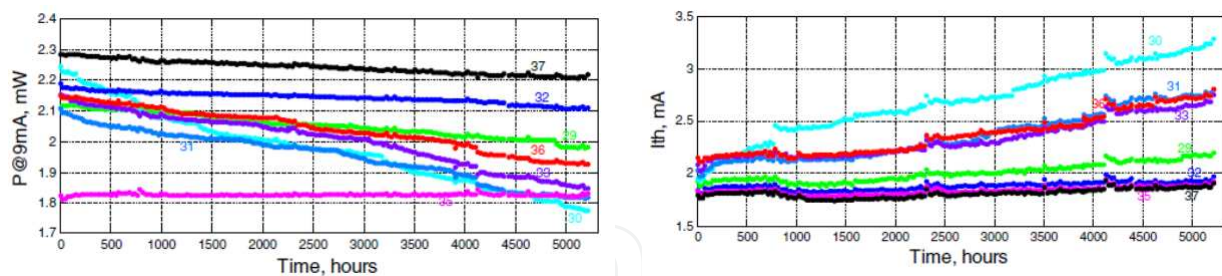
Figure 9. left: Evolution in time of emission power at 9 mA ; right: Threshold current of 8 devices under ALT test at 10 mA and temperature 150°C.

Figure 10 shows the scaled data from all ALT conditions on lognormal plots. The extracted time to 1%-failure is of 291 years at 25°C and 18 years at 70°C. With decreasing the driving currents to 8 mA and 7 mA the time to 1%-failure at 70°C increases to 30 years and 50 years respectively. These lifetime values meet the telecom industry requirements for the time to 1%-failure of more than 10 years at 70°C. In real-life applications actual lifetimes are expected to be longer since the devices spend most of the time in less demanding operating conditions. In addition, the wafer fused VCSELs have successfully passed all mechanical and electrical Telcordia qualification tests.
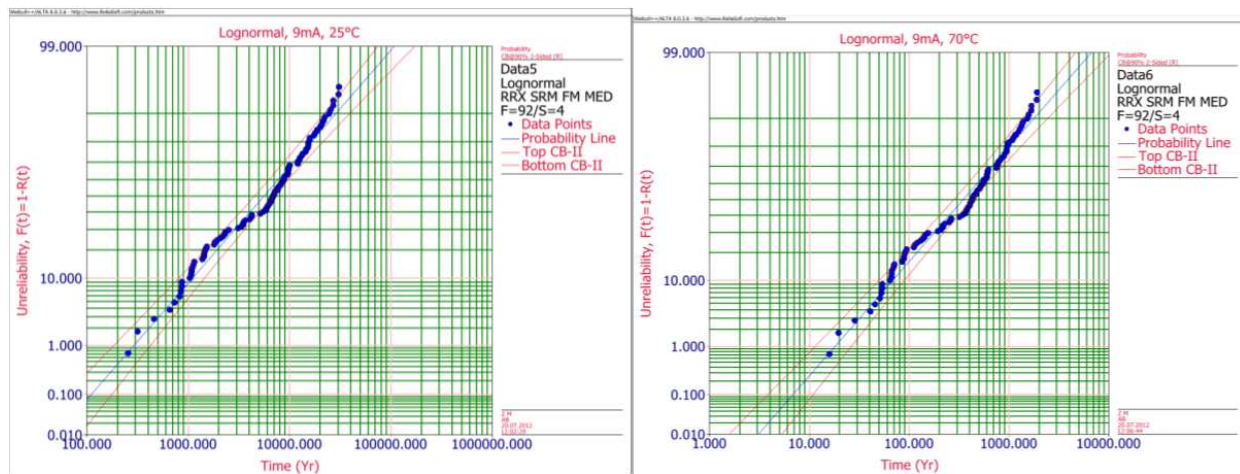
Figure 10. Lognormal plots of lifetimes (left: 25°C, right: 70°C) from the totality of test conditions scaled to an operating condition of 9 mA.

5. LW-VCSEL characterization

Below we will present typical DC and dynamic characteristics of the wafer-fused LW-VCSELs used further for processing of microwave signals. The VCSELs considered here have a device structure and performances similar to those reported in [8, 25, 26] and references therein.

5.1. Light – current characteristics

Figure 11 shows the typical light-current characteristics of the wafer fused LW-VCSELs emitting in the fundamental mode in the temperature range from 0 to 110°C. For the devices under test, the room-temperature threshold current varied from near 2 mA at 1.3 μm to less than 4 mA in 1.55-μm spectral band, and a quasi-linear dependence of optical power vs. current was observed up to 5 mW at 20°C and up to 3 mW at 70°C. Besides, room-temperature electric power consumption in quasi-linear mode is as low as 20 mW at 1.3 μm and 15 mW in 1.55-μm spectral band.

5.2. Spectral characteristics

In Figure 12 it is presented the spectral evolution of the 1560-nm VCSEL emission with current and temperature. A remarkable single-mode behavior at any of these operation conditions is observed (see also the inset of Figure 11b showing the emission spectra at room temperature and current 15 mA). As it can be easily observed, right combinations of temperature and driving current allow adjustment of the emission wavelength at any value between 1562 nm and 1572 nm. On a full wafer, VCSEL inventories of specified wavelengths can thus be selected in a quite wide spectral range of 40 nm (1550 nm to 1590 nm). A typical VCSEL spectral line shape for a 1565 nm, at 20°C and emission power 2mW is depicted in Figure 12b. As one can see, a full width at half maximum (FWHM) is as narrow as 4.5 MHz that allows VCSEL to be used effectively even in coherent fiber-optic systems.
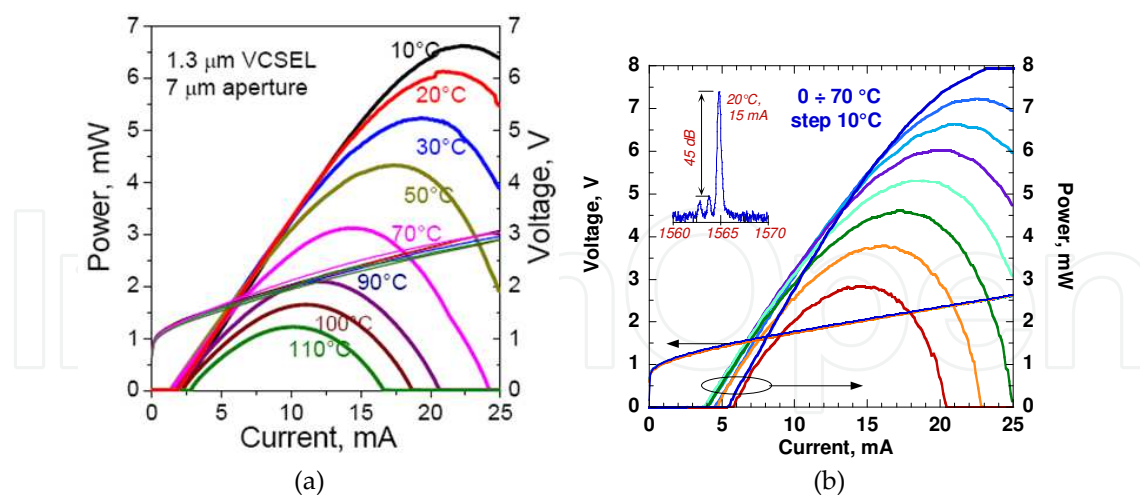
Figure 11. Light-current and volt-current characteristics of the VCSELs emitting at 1.3 μm (a) and at 1.55 μm (b)
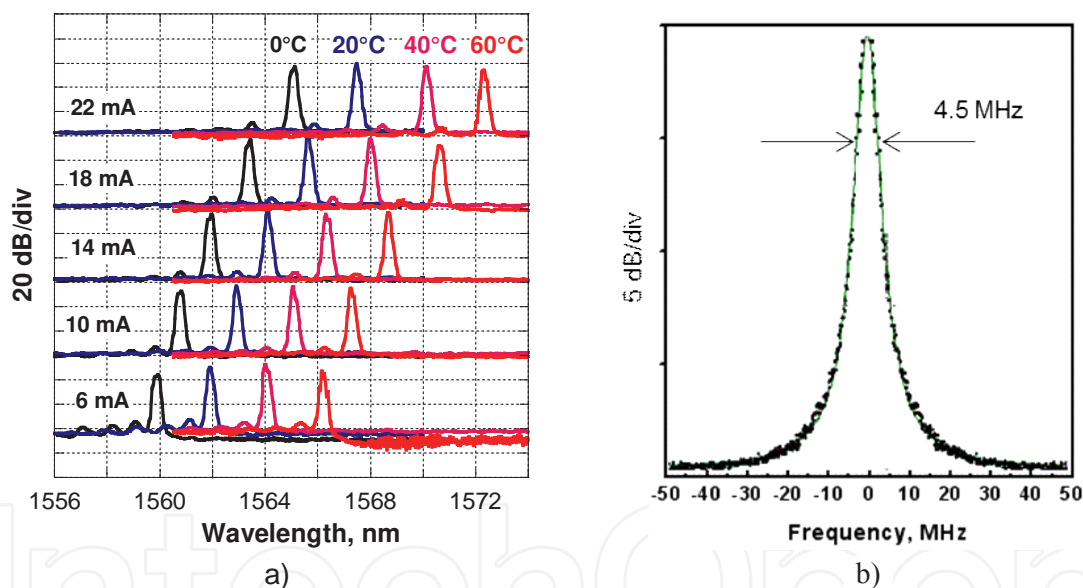

Figure 12. (a) Emission spectra of a 1560 nm VCSEL; (b) line shape of a 1565 nm VCSEL at 20°C and 2 mW emission power.

5.3. Relative intensity noise (RIN)

Figure 13 summarize the measured RIN-current characteristics of the LW-VCSELs tested at 1 and 6 GHz for the ambient temperatures of 20 and 70°C. Clearly, the RIN values decrease with increasing current and increase with increasing temperature and modulation frequency, as expected. Besides, at room temperature the RIN is as low as -160 dB/Hz (noise floor of the test setup employed) when the DC current of the laser under test is only 4.7 mA, at a modulation frequency of 1 GHz.
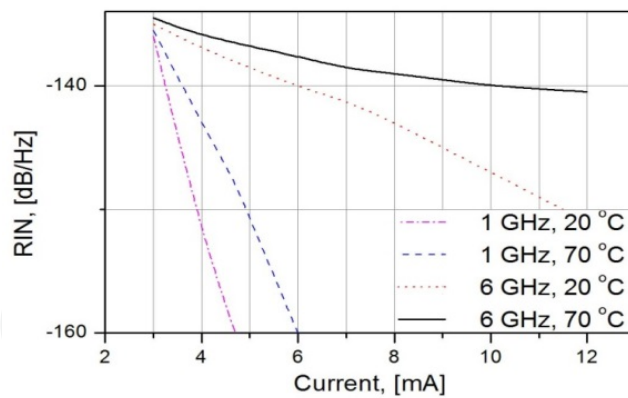
Figure 13. RIN characteristics of the wafer-fused LW-VCSELs

5.4. Small signal modulation

Figure 14 presents the small-signal transmission gain (TG) of an optoelectronic pair comprising the LW-VCSEL under test and a reference photodiode (40 GHz bandwidth, 0.6 A/W responsivity). As one can see, at lower modulation frequencies the TG value is 30 dB and the -3dB bandwidth of the LW-VCSEL under test is more than 9 GHz at 10-mA bias current.
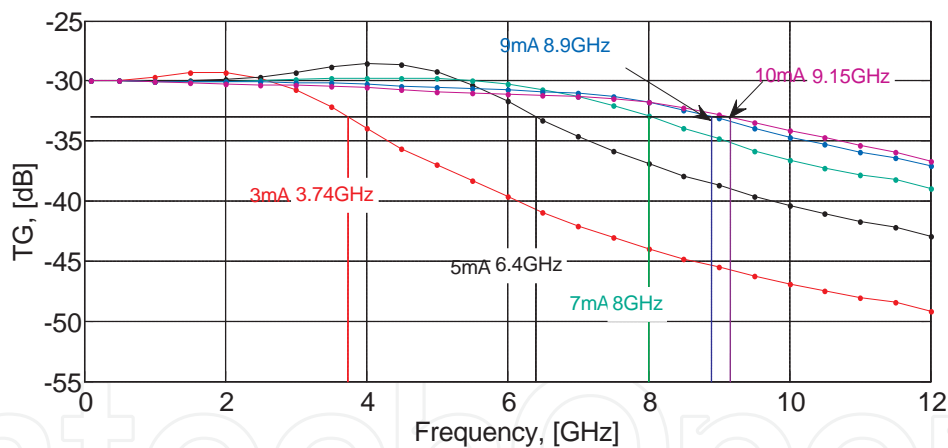
Figure 14. Small-signal transmission gain characteristics of wafer-fused LW-VCSELs

5.5. Large signal modulation

As well known, the most obvious way to assess the linear properties of an active device, in this case a semiconductor laser, is to determine its input intercept point (IIP) [27]. This parameter is most accurately determined graphically by comparing the amplitude characteristics of the laser fundamental tone and the intermodulation distortion (IMD) of corresponding order. The advantage of this parameter is the ability to compare different devices, regardless of the power of the modulating signal P_i. Simplified assessment of the third-order and fifth-order IIP (IIP3 and IIP5) values can be carried out using the following formulas:

$$IIP3 = P_i + IMD3 / 2 \tag{1}$$

$$IIP5 = P_i + IMD5 / 4 \tag{2}$$

Figure 15 depicts a typical example of IMD measurements of the tested LW-VCSELs obtained by the procedure described in [28]. Based on the measurement data and the above formulas, calculated data of *IIP3* and *IIP5* for the LW-VCSEL under test in the modulation frequency slots of 1 GHz and 6 GHz are listed in Table 2. The power of each of the input signals is P_i = 8dBm in the first frequency slot and P_i = 6dBm in the latter one.
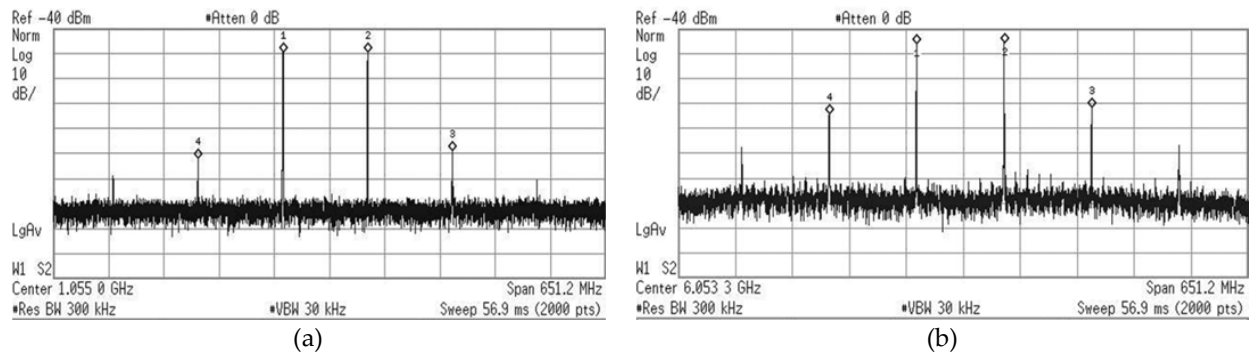
Figure 15. Measured intermodulation distortions of the wafer-fused LW-VCSELs at bias current of 9 mA in the vicinity of 1 GHz (a) and 6 GHz (b). Markers 1, 2 are the fundamental tones; markers 3, 4 are the corresponding IMD3 tones; the two extreme right and left peaks are the IMD5 tones.

Frequency [GHz]	IIP3 [dBm]	IIP5 [dBm]
1	26	20
6	20	17

Table 2. Results of calculation of IIP3 and IIP5

It follows from Table 1, that the level of *IIP*, and, therefore, the linearity of the LW-VCSELs under test, decreases with increasing modulation frequency, which agrees with other reported simulations and experimental results [28].

As mentioned above, a general figure of merit for multichannel analog optical fiber links is the SFDR that quantifies the combined effects of noise and nonlinear distortions. As shown in [29], third-order SFDR

$$SFDR = \frac{2}{3}\Big[IIP3 - EIN - 10\log\big(BW\big) \Big] \tag{3}$$

where *BW* is the system bandwidth and *EIN* is the equivalent input noise. Considering *RIN* as a predominant noise source,

$$EIN = RIN - TG \tag{4}$$

where *TG* is the transmission gain of the laser-photodiode pair (see Figure 14). The third-order SFDR is usually expressed in dB•Hz$^{2/3}$. In accordance with Figure 13, for the bias current of 10 mA that is still inside the quasi-linear regime of the light-current characteristic (Figure 11), the room temperature RIN values of the LW-VCSEL under test are below -160 dB/Hz at 1 GHz, and near -148 dB/Hz at 6 GHz. Referring to Figure 14, we find TG=-30 dB for both modulation frequencies. Using the above data and formulas, we calculate the third-order SFDR as 104 dB•Hz$^{2/3}$ for 1 GHz and 93 dB•Hz$^{2/3}$ for 6 GHz. These values are within the requirements of radio-over-fiber applications [29] in the bandwidth of 1-6 GHz, in accordance with 3GPP standard (GSM, WiFi, Bluetooth, WiMAX).

6. VCSEL-based microwave signal processing

In this section we demonstrate several examples of the application of wafer-fused LW-VCSELs for microwave analog signal processing that we have explored using VCSELs from a batch with parameters and characteristics similar to those presented in previous section.

6.1. Optoelectronic microwave signal oscillator

An optoelectronic oscillator (OEO) studied in this section is the most valuable example of microwave photonics breakthrough. As a matter of fact, OEO opens up new horizons of highly stable RF oscillators in a frequency range from 100s MHz to 100s GHz [30]. OEO has a key advantage of higher spectral purity in comparison with traditional RF and microwave oscillators [31].

The state of the art for OEOs is currently considered to be a single-frequency (within the X-band) OEO product from OEwaves Inc. [32] with a class leading phase noise level of -163 dBc/Hz at a 10 kHz offset from the carrier. The enhanced spectral purity of an OEO's central mode occurs due to its well-known feature of improving with delay time, and very long delays can be easily achieved with a nearly lossless optical fiber line extending for several kilometers. At the other hand, OEO is able to combine successfully higher spectral purity and extremely wide frequency range of carrier tuning within the limits of some octaves [33] that is impossible for traditional microwave transistor oscillators.

Up-to-date in the most publications devoted to OEO a circuit arrangement with unmodulated laser source and feedback on Mach-Zehnder external modulator has been studied. But recently a version combined the functions of optical emitter and feedback control in one vertical cavity surface emitting laser (VCSEL) preferred by potential low cost, power consumption, and integrability has been also investigated [34]. Thus, there exists a need for detailed comparison of the above OEO design approaches. Following this, below spectral and phase noise characteristics of two microwave-band OEO layouts based on an unmodulated distributed feedback (DFB) laser and an external Mach-Zehnder intensity modulator (MZM), or based on a direct modulated VCSEL will be researched and compared.

6.1.1. OE-CAD modeling

The typical layout of an OEO scheme with external modulator [35] is presented in Figure 16a. The OEO consists of two principal sections: optical and electrical. The optical section includes semiconductor laser module (SLM), electro-optical modulator (EOM), optical fiber line (OFL) and photodetector module (PDM). To ensure a reliable operation of the OEO with low laser noise levels and low loss for the optical section an optical isolator (OI) and polarization controller (PC) are introduced into the scheme. The electrical section includes a low-noise RF amplifier (LNA), tunable band-pass filter (BPF), power amplifier (PA), and electrical coupler (EC). The operating principle of the OEO is based on the conversion of the continuous optical radiation energy emitted from the SLM into periodical discrete energy bursts in the RF-band. To achieve this, the EOM is controlled by a positive-feedback optoelectronic loop (see Figure 16a). A current OEO carrier frequency in the RF band is determined by the BPF's band pass, while the overall energy storage time of OEO depends on the fiber delay. The phase and amplitude balance for self-sustained oscillations can be ensured by managing the fiber length and gain of the LNA and PA for a given circuit. The electrical section of the VCSEL-based OEO being simulated (Figure 16b) is similar to the same one of OEO with external modulator. But in optical section VCSEL is modulated directly by injection current from EC so the layout is far simpler.
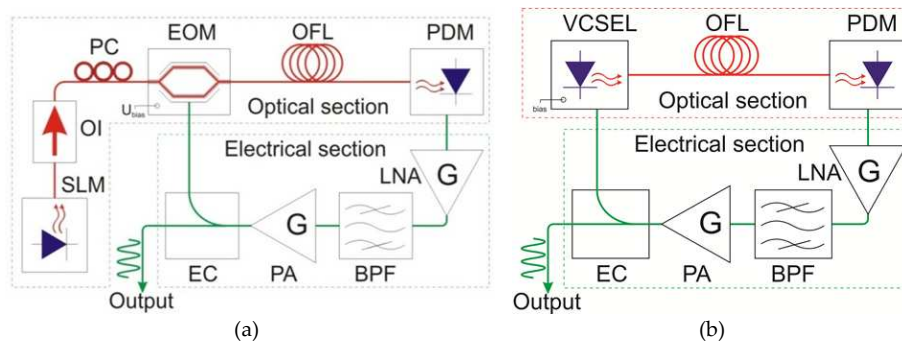

**Figure 16.** External EOM-based (a) and LW-VCSEL-based (b) OEO layouts

Previously we worked out in detail optoelectronic computer-added design (OE-CAD) based OEO model [33] by VPI System's VPI Transmission Maker software tool [36], which due to its self-excitation and large-signal steady-state operation modes allows simulating spectral and phase-noise characteristics. A single-loop EOM-based and VCSEL-based OEO computerized models are shown in Figure 17a and 17b respectively. In both cases the simulation is performed with aperiodic boundary conditions that allow concurrent simulation of the RF and optical elements of the OEO in object-oriented environment. Note that the library VCSEL model based on the rate equations does not work correctly in OEO's divergent oscillations regime, so we substituted it for a combination of equivalent laser model and ideal optical intensity modulator.

In the layouts of Figure 17 all the elements of Figure 16 have a specific interpretation. For example, the SLM is represented by single-mode rate equations-based DFB laser model, the EOM is based on a differential Mach-Zehnder interferometer model, OFL is constructed by a combination of an optical attenuator and a delay line. The spectrum of the OEO output signal

extracts by a spectrum analyzer library model. The specific schematic realization for simulating in VPI Transmission Maker OEO's phase noise characteristics in the bandwidth of 100 Hz at offsets of 10 kHz, 100 kHz and 1 MHz from the carrier, is presented in Figure 18.
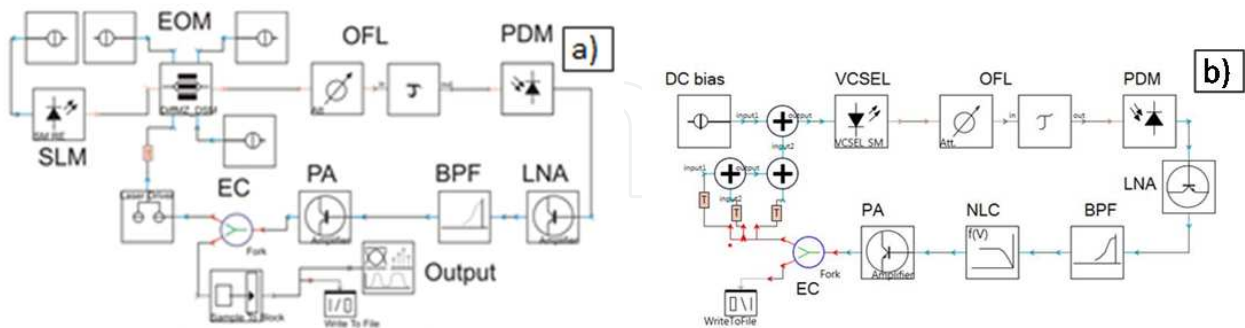
Figure 17. EOM-based (a) and VCSEL-based (b) OEO models in VPI Transmission Maker OE-CAD tool
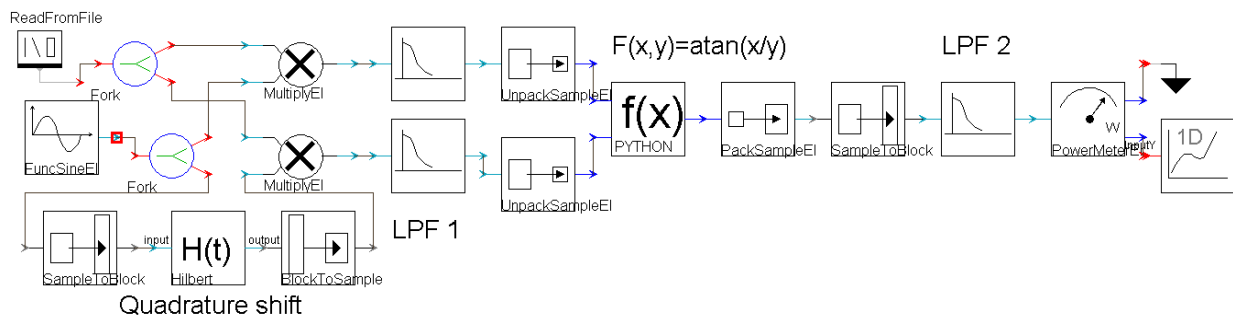

Figure 18. Arrangement for simulating OEO's phase noise measurement in VPI Transmission Maker

The simulation results of spectral and phase noise (in the bandwidth of 100 Hz) characteristics of EOM-based (a, b) and VCSEL-based (c, d) OEOs at operation frequency near 3 GHz and 65 m of OFL length are showed in Figure 19. As one can see, the both versions of OEO show comparable output powers and side-mode suppression ratios but the values of phase noise spectral density of the VCSEL-based OEO are somewhat higher.

6.1.2. Experimental verification

Experimental verification of the simulated results was performed using a prototype of the layout presented in Figure 16b. The elements employed in the optical section were: the tested wafer-fused LW-VCSEL and a pin-photodiode XPDV3120R (wavelength range 1300-1620 nm, responsivity 0.6 A/W, 3-dB bandwidth 75 GHz) from u2t Photonics, Inc. as the PDM. For the electrical section, a tunable band pass YIG-filter (tuning range 2.5-15 GHz, insertion loss 5 dB, 3-dB bandwidth 11 MHz at 2.5 GHz), from Magneton, Inc., was used as the BPF. Besides, a set of two microwave amplifiers (total gain of near 50 dB, noise figure 3.5 dB, frequency band 2.5-8 GHz) was employed.
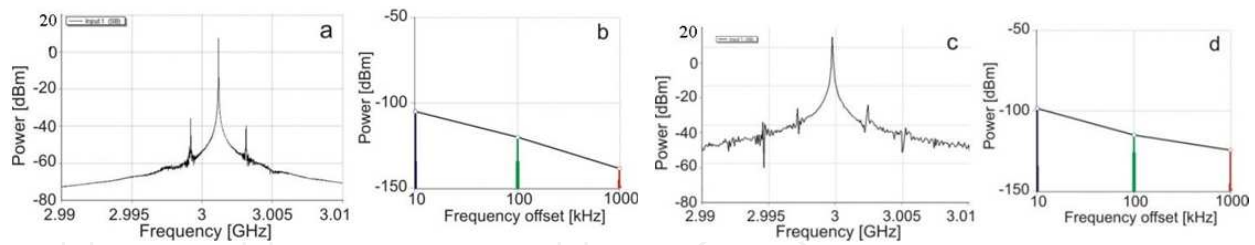
Figure 19. EOM-based OEO spectral (a) and phase noise (b) characteristics and VCSEL-based OEO spectral (c) and phase noise (d) characteristics simulated in VPI Transmission Maker OE-CAD

The examples of the experimental results of EOM-based OEO spectrum and phase noise characteristics at the oscillation frequency of 3 GHz are presented in Figures 20a and 20b [37]. In addition, the VCSEL-based OEO spectrum and phase noise characteristics at the same oscillation frequency are showed in Figure 20c and 20d.
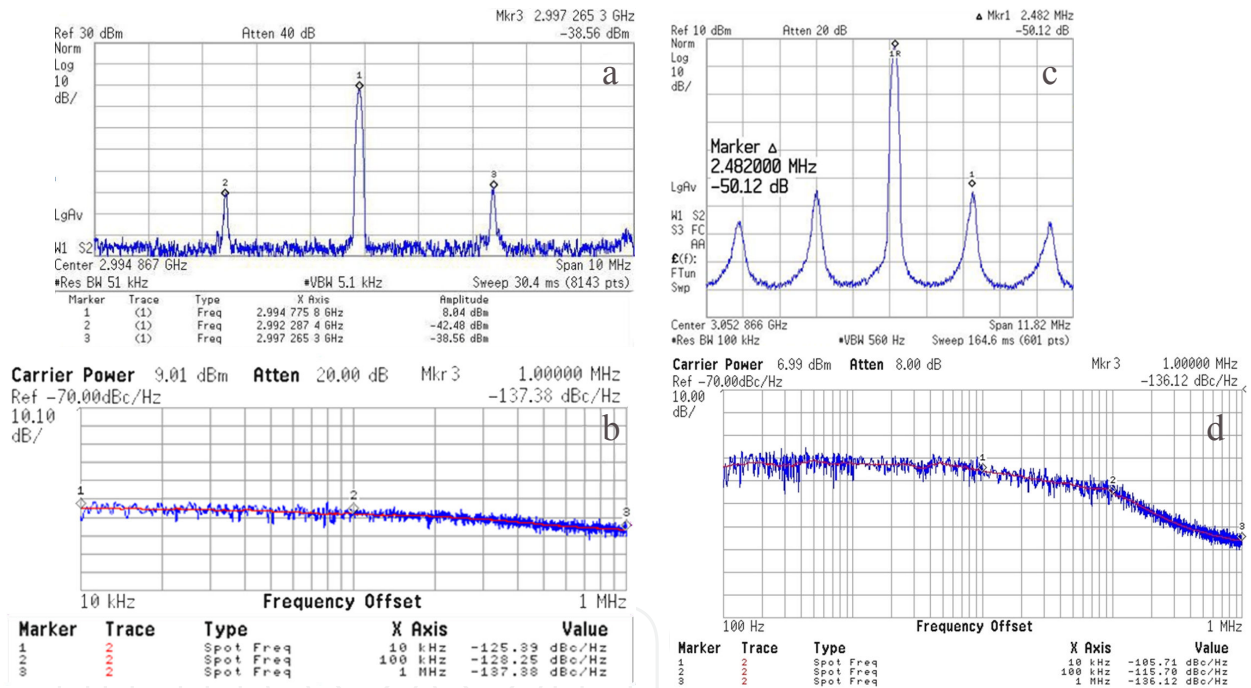
Figure 20. Measured EOM-based OEO spectrum (a) and phase noise (b) characteristics and VCSEL-based OEO spectrum (c) and phase noise (d) characteristics.

Experimental results represented in Figure 20 are closely matched with the simulation data of Figure 19 and confirm the feasibility of the proposed OEO models in VPI Transmission Maker software tool.

Table 3 presents a comparison of the VCSEL-based OEO and the one based on a distributed feedback (DFB) laser and external Mach-Zehnder intensity modulator [34, 37]. As one can see, the LW-VCSEL-based OEO exhibits similar parameters as compared to a typical EOM-based layout (except the phase noise near the carrier frequency), but also offers advantages in terms

of potential integrability, low cost and low power consumption. We believe that the most probable cause of higher phase noise of the VCSEL-based OEO is the increased relative intensity noise of the directly modulated VCSEL versus the externally modulated DFB laser. Note that a fully electronic microwave counterpart to the proposed optoelectronic solution is a phase lock loop (PLL) synthesizer. To validate the benefits of the OEO design presented here, Table 2 also lists a brief technical comparison of the OEO prototypes with IC ADF4350, an advanced wideband synthesizer with integrated voltage-controlled oscillator from Analog Devices, Inc. It is clear from the table that the LW-VCSEL-based OEO prototype provides a remarkably wide tuning range (1.5 octaves) with a comparable output power, much stronger parasitic suppression and a 14 dB lower phase noise at 10-kHz offset from the carrier.

Thus, simulating and experimental investigation of two versions of the microwave-band optoelectronic oscillator reveals that directly modulated VCSEL-based OEO, which offers a number of obvious advantages such as integrability, low cost and power consumption, has commensurable parameters compared to a typical external modulator-based layout excluding near-to-carrier phase noise. We predict that most probable cause of this defect lies in an increased radiation noise of VCSEL vs. DFB used in typical OEO layout. Another bottleneck of a VCSEL-based OEO might be the relatively limited tuning range that is referred to more narrow modulation bandwidth of the VCSEL (see Figure 14) in comparison with the same of the Mach-Zehnder modulator.

	MZM – based OEO	**VCSEL - based OEO**	ADF350 (fundamental mode)
Frequency, [GHz]	2.5-15	2.5 - 6	2.2 – 4.4
Output power, [dBm]	9	7	5
Side-mode suppression, [dB]	46.5	50	13
Phase noise at 3 GHz at Offsets, [dBc/Hz]			
10 kHz	-125	-106	-92
100 kHz	-128	-116	-111
1 MHz	-138	-136	-134

Table 3. EOM-based vs. VCSEL-based OEO comparison

6.2. Optoelectronic frequency converter and multiplicator

The microwave-band frequency conversion is usually based on the non-linear conversion features of optoelectronic devices [38], employing direct modulation of a laser [39], external modulation of passive electro-optic modulator [40, 41], semiconductor optical amplifier [38], p-i-n photodetector [42], and a combination of these components [43]. High cost and low conversion efficiency are the common drawbacks of these devices as compared with electronic

counterparts. We have analyzed the above publications and came to the conclusion that the most parametric/cost-effective technique in the case of fiber-wireless applications is direct intensity modulation of semiconductor laser, low cost emitter as LW-VCSEL, being the best candidate.

In this section, first, the details of simulation and test of VCSEL-based optoelectronic frequency mixing process are presented. Then, results of simulation and experiments of novel version of long wavelength VCSEL-based microwave frequency converter for the fiber-wireless (FiWi) base stations such as an optoelectronic sub-harmonic frequency multiplicator recently proposed [15] are presented as well.

6.2.1. Optoelectronic microwave frequency mixer

The layout of the optoelectronic frequency mixer (OE-FMX) under test realized by optical fiber means is drawn in Figure 21. Input signal (RF) and local oscillator (LO) signal are mixed in passive power combiner (PC) and directly modulate emission power of the VCSEL. An optical isolator (OI) in the layout was essential for the reliable operation of the OE-FMX with low laser noise level. Short fiber-optic patchcords, p-i-n photodiode (PD) and band-pass filter (BPF) are the main elements of optical path for optical emission (modulated by the complex RF+LO signals) propagation, detection and converted frequency output selection, respectively.
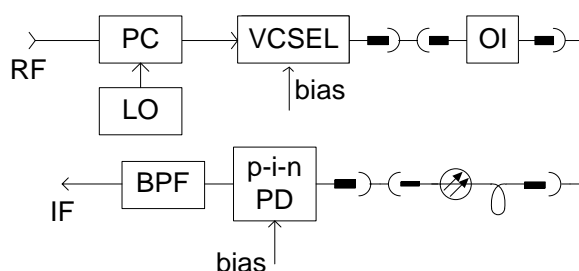
Figure 21. Layout of the long wavelength VCSEL-based optoelectronic frequency mixer under test

A modeling of the parameters of both devices characterized in the section was also performed by the same OE-CAD as for OEO. In this tool the library VCSEL model is addressed to single-mode rate equations and calibrated based on the measured light-current and small-signal modulating plots (see Figures 11, 14). A schematic layout of the computerized model is depicted in Figure 22 for the OE-FMX block diagram shown in Figure 21. For better visualization, the circuitry does not include a model of BPF with a central frequency of 2.5 GHz. Simulation details are reported in [15, 44].

The conversion efficiency (CE) is studied by simulation. In this case this is the difference (in dB) between IF signal power on the BPF (or PD) output and the RF signal power on the VCSEL's modulating input. Figure 23 presents the simulated (a) and PSA-measured (b) OE-FMX output spectra with up-conversion of L to S microwave bands. In both cases the input RF signal had a power of -20 dBm at 1 GHz and LO signal had a power of 6 dBm at 1.5 GHz.

At VCSEL DC bias current of 7 mA an output (IF) signal power near -55 dBm at a frequency of 2.5 GHz, i. e. CE of -35 dB was measured. The good fit of the experimental and simulation results confirm the feasibility of the proposed OE-FMX model.
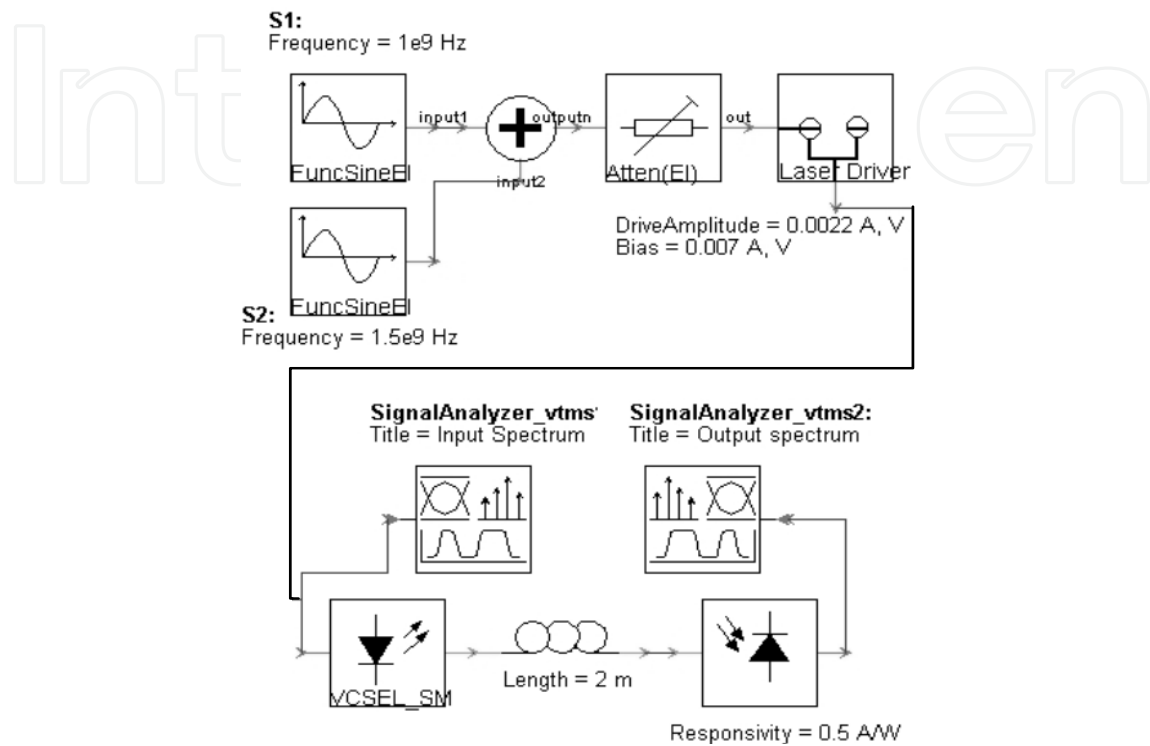

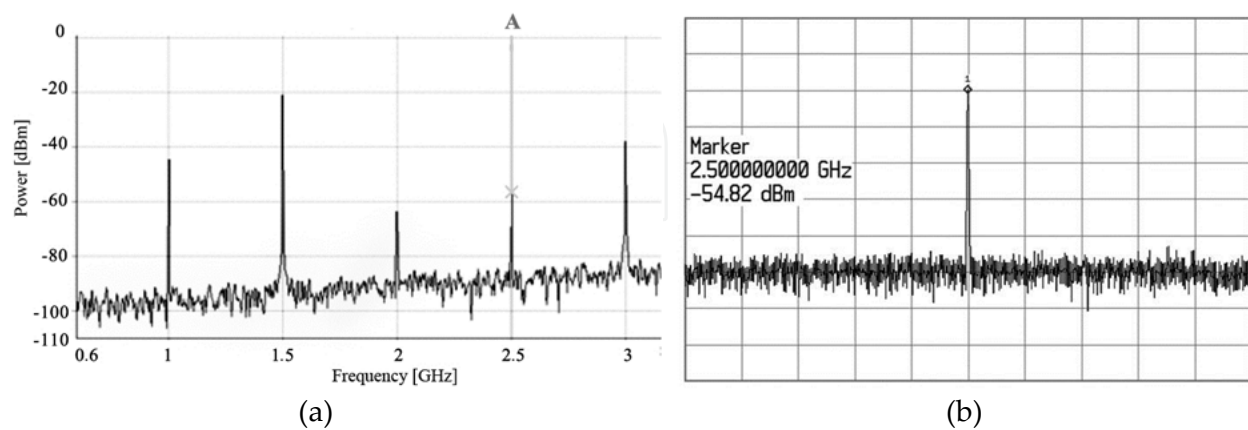**Figure 22.** OE-CAD model of the OE-FMX under test

Figure 23. Simulated (a) and PSA-measured (b) OE-FMX output spectra with up-conversion of L to S microwave bands

It is clear that CE vs. frequency plot of this device is in line with the modulation characteristic of the tested VCSEL (see Figure 14). The results of prototyping the rest inherent characteristics

of long wavelength VCSEL-based OE-FMX under test such as CE vs. input and local oscillator power, second-order and third-order IIP, and VSWR, are depicted in Figures 24-27.

The outcome of Figure 24 is that the input linearity threshold (P_{-1dB}) is near 2 dBm, that is comparable with standard transistor microwave mixer. Besides, Figure 25 shows the conversion efficiency to be remarkably local power-selective and its maximum value is near -33 dB at power as low as 3 dBm. To complete checking in accordance to traditional microwave mixers the tests of input second-, third-order intercept points (IIP2, IIP3) and voltage standing wave ratios (VSWR) for the OE-FMX prototypes are demonstrated (Figure 26). At the result, IMD values coincide exactly with the same for intrinsic VCSEL measurement (see Figure 15, Table 2), that makes clear that VCSEL is the most nonlinear element of OE-FMX layout. Additionally, VSWR values for RF and LO inputs and IF outputs (Figure 27) are lower than 1.7 within the bandwidth of 0.5-8 GHz.

6.2.2. Optoelectronic microwave frequency multiplicator

In ref. [15] we have proposed and investigated a simplified version of OE-FMX, the optoelectronic frequency multiplicator (OE-FMP) with the goal of achieving higher cost-efficiency of the VCSEL-based OE-FMX. Its block diagram is similar to that of Figure 16, but without power combiner and local oscillator. The principle of the approach is based on using the effect of a period doubling [45] under modulation of a semiconductor laser by a power RF sinusoidal signal. For this purpose, the laser should be modulated in super large-signal mode with an injection current cutoff similar to a class C regime in electronic amplifier. To reach this regime, the laser bias current has to be set in a near-threshold (but higher) area or in the onset of quasi-linear zone of the laser's light-current plot. In this regime inside the laser optical emission spectrum some sub-harmonics and the products of their mixing with the above tones are generated, in addition to fundamental frequency and its higher harmonic tones. In simulation we succeeded in identification of such a regime of semiconductor laser, where the signal levels of a fundamental modulation frequency F, a sub-harmonic tone 0.5F, and a component at 1.5F would be near equal and enough to secure the signal-to-noise ratio needed for wireless communication systems.
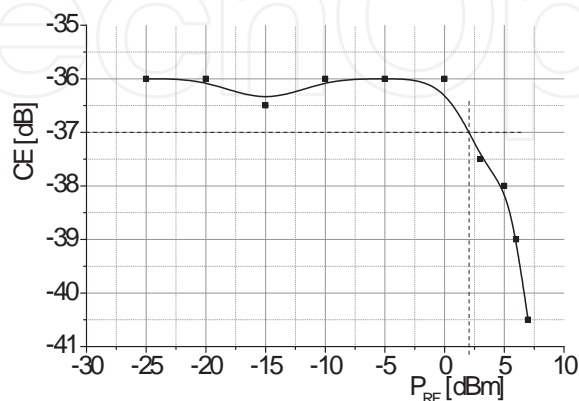
Figure 24. Conversion effectiveness vs. RF signal power (P_{LO}=6 dBm)
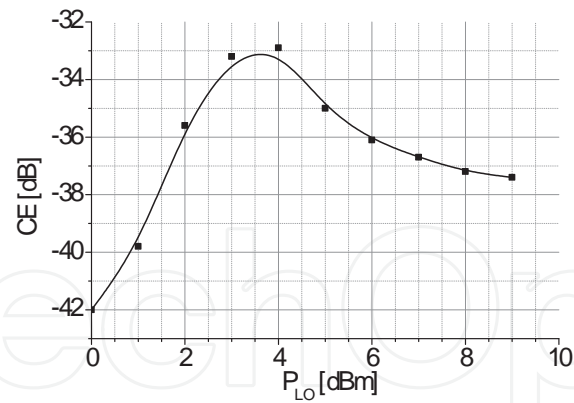
Figure 25. Conversion effectiveness vs. local oscillator power (Ps=-20 dBm)
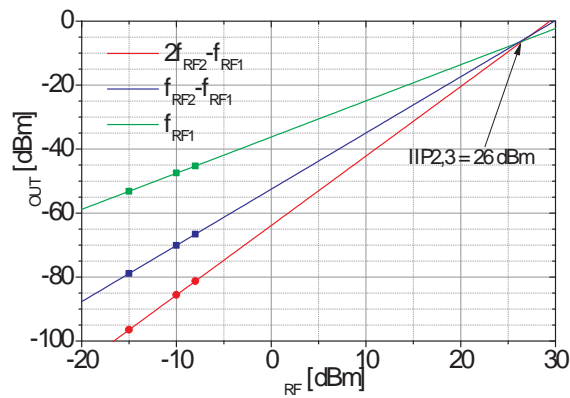
Figure 26. Second (IIP2) and third (IIP3) order input intercept points
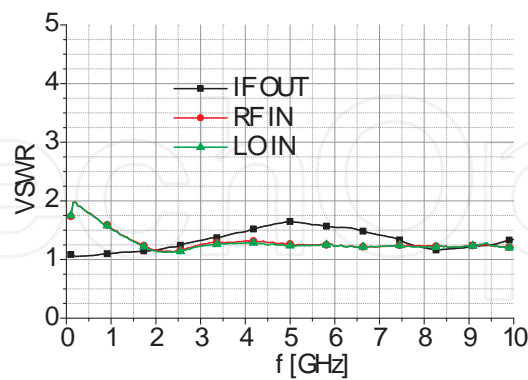
Figure 27. Input and output voltage standing-wave ratio (VSWR)

6.2.2.1. Formal-oriented VCSEL model in super large-signal mode

As it is well-known, for example, see [46], a system of rate equations is used to address the dynamic operation of a single-mode MQW semiconductor laser, in our case, of a VCSEL. The

main issue is in identification of the necessary operating range for the VCSEL under investigation, because the nonlinear rate equations do not always converge to the desired solution. To address this issue, a preliminary computation by MathCAD tool was performed, with a restrictive condition that the difference of fundamental and nearest sub-harmonic or mixed tones must be below 10 dB. The results are depicted in Figure 28. The area 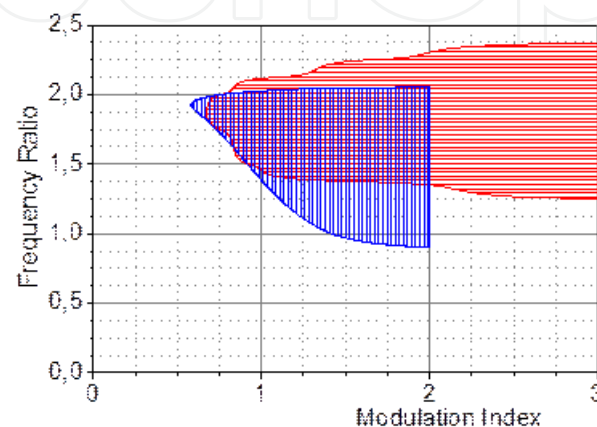with horizontal hatching is of the operation area of VCSEL's effective functioning in the sub-harmonic multiplication regime.
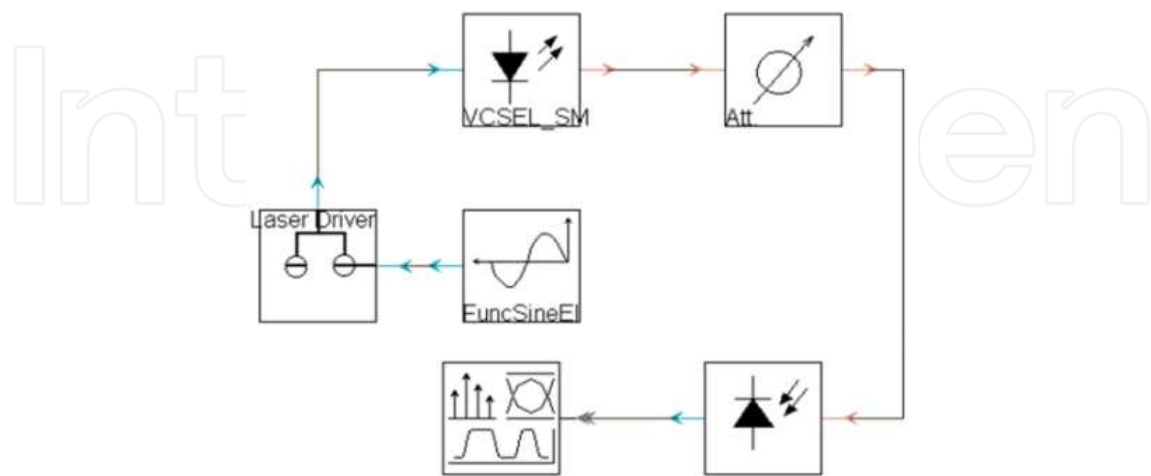

Figure 28. Diagram for the validating the VCSEL's effective functioning in the sub-harmonic multiplication regime

The terms "Frequency ratio" and "Modulation Index" (Figure 28) mean an input RF frequency normalized by the laser's small-signal resonance one, and AC modulation current amplitude normalized by the laser's DC bias current, respectively. As one can see, effective process of generating nearest to fundamental frequency sub-harmonic or mixed tones is obtained when a modulation frequency is higher than a laser's relaxation frequency (RFQ) and even higher than its 3-dB direct modulation bandwidth as well as when the current modulation index is more than 0.7; in good agreement with known data. The simulation results of the period doubling effect for an edge-emitted laser [45] (Figure 28, vertical hatching) show large overlapping of the areas with horizontal hatching, that confirms validity of the developed model.

6.2.2.2. OE-FMP's object-oriented modeling, verification and example of realization in FiWi network

Simulation data presented in Figure 28 became the basis for the modeling of optoelectronic microwave frequency multiplicator by the same OE-CAD tool as for OE-FMX. The developed object-oriented model is presented in Figure 29. All labels are the same as for Figure 22. A number of simulation experiments were performed on this model with a goal of choosing the optimal regime for each given device. The simulated (a) and PSA-measured (b) OE-FMP output spectra together with input microwave-band frequency are presented on Figure 30. For both procedures the input RF signal was kept at 0 dBm power level at a frequency F=3 GHz and VCSEL DC bias current was set at 3.2 mA. As one can see, the experimental results fit well

with the simulation results thus validating the proposed OE-FMP model. The rest of the parameters of the OE-FMP prototype coincide with the same ones for the OE-FMX.

Figure 29. VPI transmission Maker™ object-oriented model of the OE-FMP

Marker	X Axis	Amplitude
1	1.5 GHz	-42.23 dBm
2	3.0 GHz	-44.17 dBm
3	4.5 GHz	-45.88 dBm
4	6.0 GHz	-52.27 dBm

(a)   (b)
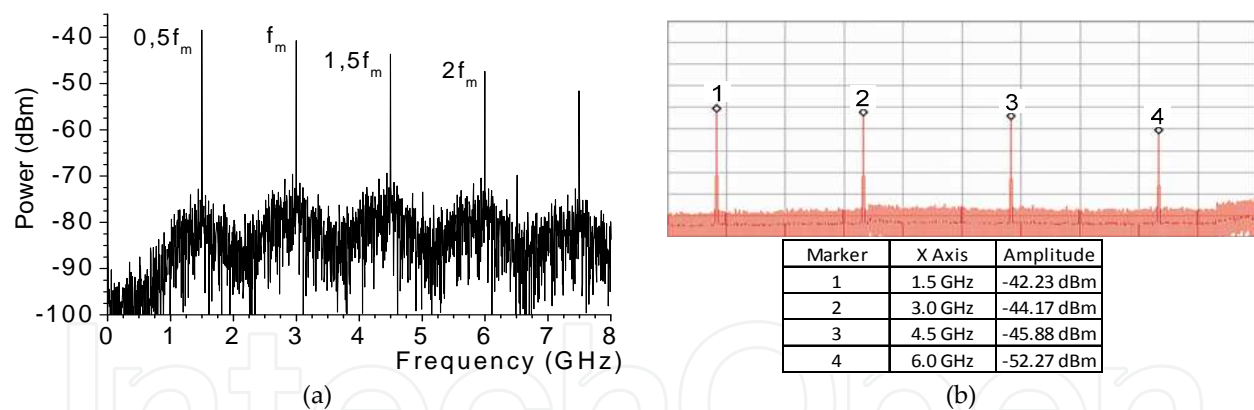
Figure 30. Simulated (a) and measured (b) output spectra of VCSEL-based OE-FMP.

Since a practical application of the developed OE-FMP is not as clear as a microwave-band optoelectronic frequency mixer, below a version of its effective realization in an advanced telecom system based on Radio-over-Fiber (RoF) technology is exemplified [47]. Hybrid Fiber-Wireless (FiWi) access network is a novel backhaul network architecture that integrates the next-generation WLAN-based wireless mesh network and Ethernet passive optical network (EPON). Its major feature lies in squeezing the cell diameters up to picocell (10s - 200 m) or femtocell (10s cm – 10s m) [48]. As a result the base station equipment must satisfy extremely rigid requirements related to the cost-effectiveness. To meet this issue we propose to use OE-FMP described beyond in the base station's uplink channel that is much simpler than the

known methods using a microwave local oscillator or remote delivery of a reference oscillator signal [49]. Figure 31 shows an example of uplink circuitry realization by the OE-FMP in the popular X-band. The rest elements of the layout are: 1 - receiving antenna, 2 – sub-harmonically pumped mixer, 3 – IF filter, 4, 7 – amplifier, 5 – coupler, 6 – uplink laser, 8 – carrier recovery unit. The main benefits of the layout proposed are: (i) in realistic simplification of the base station arrangement without the concurrent complication of a central office architecture or remote delivery of oscillator signal as in known approaches; (ii) in improvement of a base station's cost features; (iii) in coarser demands to local oscillator frequency stability.
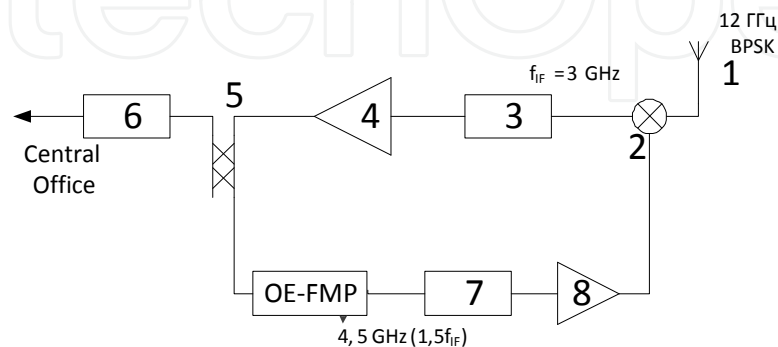
Figure 31. Example of OE-FMP application in uplink channel of FiWi network

Above, a detailed investigation of two low cost VCSEL-based microwave photonics devices: known optoelectronic frequency mixer and novel sub-harmonic frequency multiplicator for the circuitry of FiWi's base stations is presented. The main advantage of using optoelectronic approach in general and VCSELs in particular is in:

- Large bandwidth, that is limited by the bandwidths of laser and photodiode solely,

- Application versatility, the same block diagram for up-converter and down-converters

- Losses do not depend on a position of microwave frequencies inside the operation band, as compared with the inherent effect of increasing conversion loss with a super wide frequency of a microwave transistor mixer.

- Design simplicity (practically decoupled input and output),

- Lower power consumption (5-10-fold lower than edge-emitting laser), and

- Lower required output power of the local oscillator (only some dBm instead of 15-20 dBm for edge-emitting laser).

Table 4 lists a summary of the results referred to demonstrated LW-VCSEL-based devices for frequency converting microwave signals [44]. As seen, simulation and experimental values are rather close.

Altogether, the microwave photonics frequency conversion devices based on LW-VCSEL demonstrate a remarkable potential for the application in future equipment for ultra-wide band telecom and radar systems. (in phased-array antenna systems, measurement techniques, to name only a few). The work is in progress for decreasing conversion losses in these devices.

		Operating bandwidth [GHz]	LO power [dBm]	Conversion efficiency [dB]	P-1 dB [dBm]	**IIP2 [dB]**	IIP3 [dB]	IIP5 [dB]
OE-FMX	Theory	6	6	-36	-	-	25, 5	19, 2
	Experiment	5, 5	4	-33, 2	2	26	26	20
OE-FMP	Theory	1, 2...2, 5	-	-42, 0	-	-	25, 5	19, 2
	Experiment	1, 4...2, 4	-	-45, 0	-	26	26	20

		VSWR			Input/output isolation [dB]				NF [dB]
		RF input	LO input	IF output	LO-IF	2RF-IF	RF-IF	LO-RF	
OE-FMX	Theory	1*	1*	1*	26	44	25	∞*	-
	Experiment	1, 5	1, 3	1, 3	33	39	32	15	34
OE-FMP	Theory	1*	-	1*	-	48	41	-	-
	Experiment	1, 7	-	1, 3	-	52, 3	44, 2	-	44

*Ideal elements were used

Table 4. Summary of the results referred to developed LW-VCSEL-based devices for frequency converting microwave signals

7. Challenges in LW-VCSEL photonics

In the sections above we have demonstrated the potential of the long-wavelength low power consumption VCSELs for microwave photonics applications. Further development will make available such VCSELs with increased performances and lower power consumption thus allowing implementation of VCSELs in optical integrated circuits [10] and realization of new functionalities as VCSEL-based optical frequency combs [51]. Altogether such development will pave the way to photonic microwave transistor [52]. At the same time, a major shortcoming of VCSEL compared with DFB laser is its relatively low emitting power that constrains its penetration, for example, into telecom multi-branch passive optical networks (PON), and into transmission units of processing circuitry with external modulation by higher loss MZM. One of possible solution to overcome it is using vertical external cavity surface emitting lasers (VECSEL). Besides obvious fiber-optics applications in optical communications and optical clocking in supercomputers, VECSELs emitting in this wavelength range presents interest also in MWP [53]. Very recently, two-color tunable VECSEL with various gain chip configuration have demonstrated a wavelength separations ranging from nearly zero to more than two hundred nanometers [54]. Watt-level semiconductor disk lasers (SDL) emitting in the 1300 nm band were demonstrated using the wafer fusion fabrication technique [55, 56]. In [58] it is reported the state of the art in design and performance of electrically pumped VECSEL in 14XX nm band produced by the wafer fusion technique that exhibits 6.2 mW output power in continuous wave operation.

8. Conclusion

In this chapter a number of author's original works in the area of long-wavelength wafer-fused vertical channel surface emitting laser design, fabrication, and application is reviewed. Specifically, design, fabrication, DC and dynamic performances and a special benefit of wafer-fused LW-VCSELs for microwave photonic devices are highlighted. As described, wafer fused LW-VCSELs exhibit the above-listed unique features that might pave the way for their exploitation in future telecom and radar modules based on microwave photonics technology. The validity of this statement is supported both through the proper transmission characteristics of the wafer-fused LW-VCSEL itself and by simulation and experimental results of a number of basic microwave photonics devices presented here: an optoelectronic microwave-band oscillator, two versions of optoelectronic microwave-band frequency converters. Besides the above-described applications, some other examples of important microwave photonic devices based on LW-VCSELs have been published, for example in heterogeneous silicon photonic integrated circuits [10], coherent transmission module of the PON's upstream channel [50], and optical frequency comb generators [51]. Also, as a newer trend of VCSEL photonics, some recent author's investments referred to vertical external cavity surface emitting laser (VECSEL) are discussed. All these examples clearly testify that LW-VCSELs themselves and microwave photonics devices based on them have a great potential in future telecom and radar systems both for civil and for military applications.

Author details

M. E. Belkin[1*], L. Belkin[1], A. Loparev[1], A. S. Sigov[1] and V. Iakovlev[2]

*Address all correspondence to: belkin@mirea.ru

1 Moscow State Technical University of Radio-Engineering, Electronics and Automation (MIREA), Moscow, Russia

2 Ecole Polytechnique Fédérale de Lausanne (EPFL), Switzerland

References

[1]   Seeds A. J., Williams K. J. Microwave Photonics. IEEE Journal of Lightwave Technology 2006; 24(12) 4628-4641.

[2]   Kapon E., Sirbu A. Long-wavelength VCSELs: Power-efficient answer. Nature Photonics 2009; 3, 27-29 doi:10.1038/nphoton.2008.266.

[3] Belkin M. E., Belkin L., Loparev A.,. Sigov A. S, Suruceanu G., Sirbu A., Mereuta A., Caliman A., Ellafi D., Iakovlev V., Kapon E. VCSEL-based Processing of Microwave Signals. 2014; DOI: 10.1109/MWP.2014.6994554 ;

[4] Charlier J. C., and Krüger S. Long-wavelength VCSELs ready to benefit 40/100-GbE modules. Lightwave, 2012; http://www.lightwaveonline.com/articles/print/volume-28/issue-6/technology/longwavelength-vcsel-technology-improves.html.

[5] Yao J. Microwave Photonics. IEEE Journal of Lightwave Technology 2009. 27(3) 314.

[6] Capmany J., Novak D. Microwave photonics combines two worlds. Nature Photonics 1, 319-330 doi:10.1038/nphoton.2007.89

[7] Koyama A. F. Recent advances of VCSEL photonics. IEEE Journal of Lightwave Technology 2006.24(12) 4502-4513.

[8] Sirbu A., Iakovlev V., Mereuta A., Caliman A., Suruceanu G. and Kapon E.Wafer-fused heterostructures: application to vertical cavity surface-emitting lasers emitting in the 1310 nm band. Semicond. Sci. Technol. 2011.26(1) 014016.

[9] Chrostowski L., Chang C-H., and Chang-Hasnain C. J. Enhancement of dynamic range in 1.55-um VCSELs using injection locking. IEEE Photon. Technol.Lett. 2003.15(4) 498-500.

[10] Miller D. A. B. Device Requirements for Optical Interconnects to Silicon Chips. Proceedings of the IEEE 2009.97(7) 1166-1185

[11] Michalzik R. Fundamentals, Technology and Applications of Vertical-Cavity Surface-Emitting Lasers. Springer Series in Optical Sciences 166;2013.

[12] Shau R., Ortsiefer M., Rosskopf J., Böhm G., Lauer C., Maute M., Amann M.-C. Long-wavelength InP-based VCSELs with buried tunnel junction: properties and applications. Proceedings of SPIE 2008; 5364, 1–15.

[13] Caliman A., Mereuta A., Suruceanu G., Iakovlev V., A. Sirbu et al. 8 mW fundamental mode output of wafer-fused VCSELs emitting in the 1550-nm band. in Optics Express 2011;19(18) 16996.

[14] Gamage P. F., Nirmalathas A. Performance comparison of directly modulated VCSEL and DFB lasers in wired-wireless networks. IEEE Phot. Technol. Lett. 2008;20(24) 2102-2104.

[15] Belkin M. E., Belkin L. M. Microwave-Band Optoelectronic Frequency Converters Based on Long Wavelength VCSELs. IEEE COMCAS 2011: conference proceedings, 7-9 November, 2011, Tel Aviv.

[16] Baecker A. Transverse optical mode analysis of long-wavelength VCSEL in high single-mode operation. Proc. 8th Int. Conf. of Numerical Simulation of Optoelectronic Devices (NUSOD) 2008:conference proceeding, p. 87.

[17] Sirbu, A., Suruceanu, G., Iakovlev, V., Mereuta, A., Mickovic, Z., Caliman, A., Kapon, E. Reliability of 1310 nm Wafer Fused VCSELs. IEEE Phot. Technol. Let. 2013; 25(16)1555-1558.

[18] Sirbu A., Mereuta A., Caliman A., Iakovlev V., Suruceanu G., Ellafi D., Mickovic Z., and Kapon E. Wavelength controlled VCSELs emitting in the 1310-nm waveband. SPIE Photonic Europe 2014: conference proceedings, April, 14-17 2014, Brussels.

[19] Iakovlev V., Suruceanu G., Caliman A., Mereuta A., Mircea A., Berseth C.-A., Syrbu A., Rudra A., and Kapon E. High-performance Single Mode VCSELs in the 1310-nm Waveband. IEEE Photonics Technol. Lett. 2005; 17(5) 947 – 949.

[20] Mereuta A., Syrbu A., Iakovlev V., Rudra A., Caliman A.et al. 1.5μm VCSEL Structure Optimization for High Power and High Temperature Operation. J. Crystal Growth 2004; doi:10.1016/j.jcrysgro.2004.08.034

[21] Mereuta A., Sirbu A., Caliman A., Suruceanu G., Iakovlev V., Mickovic Z., Kapon E. Fabrication and performance of 1.3-μm 10-Gb/s CWDM wafer-fused VCSELs grown by MOVPE. Journal of Crystal Growth 2014; doi:10.1016/j.jcrysgro.2014.11.012.

[22] Sirbu A. and Kapon E. Ultra-Low Power VCSELs for optical network. Compound semiconductors 2013; June, p. 41-44.

[23] Information SuperStore : http:.telecominfo.telcordia.com/ido/AUX/ GR_468_TOC.i02.pdf. (accessed 25 /01/ 2015).

[24] Rhew K. H., Jeon S. C., Lee D. H., Yoo B.-S., and Yun I. Reliability assessment of 1.55-μm vertical cavity surface emitting lasers with tunnel junction using high-temperature aging tests. Microelectron. Rel. 2009; 49(1) 42–50.

[25] Iakovlev V., Sirbu A., Mickovic Z. et al. Progress and challenges in industrial fabrication of wafer-fused VCSELs emitting in the 1310 nm band for high speed wavelength division multiplexing applications. Proc. of SPIE 2013; 8639, 863904-1 - 863904-7.

[26] Caliman A., Mereuta A., Suruceanu G., Iakovlev V., Sirbu A. et al. 8 mW fundamental mode output of wafer-fused VCSELs emitting in the 1550-nm band. Optics Express 2011;19(18)16996.

[27] Pedro J. C., Carvalho N. B. Intermodulation Distortion in Microwave and Wireless Circuits. Artech House, Inc., London; 2003.

[28] Belkin M. E., Belkin L. et al. Performances of Microwave-Band Analog Signal Transmission using Wafer-Fused Long Wavelength VCSELs. IEEE Phot. Technol. Lett. 2011; 23(20)1463-1465.

[29] H. Al-Raweshidy, S. Komaki, Radio over fiber technologies for mobile communication networks. Artech House, 2002.

[30] Yao X. S. Opto-electronic Oscillators. In: W. S. C. Chang (ed.) RF Photonic Technology in Optical Fiber Links. Cambridge University Press;2002. 255-292.

[31] Maleki L. Recent Progress in Opto-Electronic Oscillator, in conference proceedings: Microwave Photonics International Topical Meeting 2005, DOI: 10.1109/MWP. 2005.203545

[32] http:.www.oewaves.com

[33] Belkin M.E., Loparev A.V., Semenova Y. et al. A Tunable RF-Band Optoelectronic Oscillator and OE-CAD Model for its Simulation. Microwave and Optical Technology Letters 2011;53(11)2474-2477.

[34] M. E. Belkin, and A.V. Loparev. "A Microwave Optoelectronic Oscillator: Mach-Zehnder Modulator or VCSEL Based Layout Comparison", *PIERS Proceeding*, pp. 1138-1142, Moscow, 2012.

[35] Yao X.S., Maleki L. Optoelectronic oscillator for photonic systems. IEEE Journal of Quantum Electronics 1996; 32(7) 1141-1149.

[36] http:.www.vpisystems.com

[37] Loparev A. V. Optoelectronic and Microelectronic Building Principles of Solid-State Microwave Oscillators, PhD thesis. MSTU MIREA; 2011.

[38] Cabon B., Le Guennec Y., Lourdiane M., and Maury G. Photonic mixing in RF modulated optical link, in LEOS 2006, Oct. 2006, pp. 408-409. DOI: 10.1109/LEOS. 2006.279173

[39] Constant S. B., Le Guennec Y., Maury G., Corrao N., and Cabon B. Low-cost all-optical up-conversion of digital radio signals using directly modulated 1550-nm emitting VCSEL. IEEE Photonics Technol. Lett. 2008; 20(2)120-122.

[40] Lindsay A. C., Knight G. A., and Winnall S. T. Photonic Mixers for Wide Bandwidth RF Receiver Applications. IEEE Trans. on MTT 1995;43(9)2311-2317.

[41] Polo V., Marti J., Ramos F., Fuster J. M. Millimetre-wave Optical Harmonic Mixer Employing a Sigle Mach-Zehnder Electro-Optic Modulator. 28th European Microwave Conference;1998 DOI: 10.1109/EUMA.1998.338096

[42] Malyshev S. A., Chizh A. L. P-i-n Photodiodes for Frequency Mixing in Radio-over-Fiber Systems. IEEE J of Lightwave Technol. 2007; 25(11) 3236-3243.

[43] Cabon B. Microwave Photonics Mixing. Transactions D: Computer Science & Engineering and Electrical Engineering 2010;17(2) 149-162

[44] Belkin L. Microelectronic and optoelectronic design principles of microwave semiconductor frequency converters. PhD Thesis. MIREA, Moscow; 2012.

[45] Hemery E., Chusseau L., and Lourtioz J.-M. Dynamic Behaviors of Semiconductor Lasers under Strong Sinusoidal Current Modulation: Modeling and Experiments at 1.3 μm. IEEE J of Quantum Electron.1990; 26 (4) 633-641.

[46] Piprek J., Bowers J. E. Analog modulation of semiconductor lasers. In: Chang W. S. C. (ed.) RF Photonic Technology in Optical Fiber Links. Cambridge University Press; 2002.p 57-79.

[47] Belkin M. E.and Belkin L. M. Method and apparatus of base station building for RoF-structured telecom system. RF Patent No 2472290, priority from July, 11, 2011.

[48] Sauer M., Kobyakov A., George J. Radio over Fiber for Picocellular Network Architectures. IEEE J of Lightwave Technol. 2007; 25(11) 3301-3320

[49] Kaszubowska A., Hu L. Barry L. P. Remote Downconversion with Wavelength Reuse for the Radio/Fiber Uplink Connection. IEEE Photonics Technol. Lett. 2006;18(4)562-564.

[50] Olmos J. J. V., Rodes R., Monroy I. T. Low power consumption O-band VCSEL sources for upstream channels in PON systems. in *Proc. OECC*, pp. 130-131, Jul. 2012; DOI: 10.1109/OECC.2012.6276405

[51] Serrano A. C., Fernandez C. de Dios et al. VCSEL-Based Optical Frequency Combs: Toward Efficient Single-Device Comb Generation. IEEE Photonics Technol. Lett. 2013;25(20)1981-1984.

[52] Pérez D., Gasulla I. and Capmany J., Microwave Photonics Transistor Design Equations, 2014 International Topical Meeting on Microwave Photonics (MWP) and the 2014 9th Asia-Pacific Microwave Photonics Conference (APMP), p.82, DOI: 10.1109/MWP.2014.6994496.

[53] Kuznetsov M.VECSEL Semiconductor Lasers: A Path to High-Power, Quality Beam and UV to IR Wavelength by Design. In Semiconductor Disk Lasers: Physics and Technology, Prof. Dr. Oleg G. Okhotnikov. Published Online: 16 JUL 2010, DOI: 10.1002/9783527630394.ch1

[54] Lukowski M., Hessenius C., Fallahi M.. Widely Tunable High-Power Two-Color VECSELs for New Wavelength Generation. IEEE J. OF SELECTED TOPICS IN QE 2015;21(1), 1700208

[55] Rantamäki A., Sirbu A., Saarinen E., Lyytikäinen J., Mereuta A., Iakovlev V., Kapon E., and Okhotnikov O., High-power flip-chip semiconductor disk laser in the 1.3um wavelength band. Opt. Lett.2014; 39(16), 4855-4858.

[56] Sirbu A., Rantamäki A., Saarinen E. J., Iakovlev V., Mereuta A. et al. High performance wafer-fused semiconductor disk lasers emitting in the 1300 nm waveband. Optics Express 2014;22(24) 29398

[57] Iakovlev V., Walczak J., Gebski M., Sokol A. K., Wasiak M. et al. Double-diamond high-contrast-gratings vertical external cavity surface emitting laser. Journal Of Physics D-Applied Physics 2014;47(6).

[58] Caliman A., Sirbu A., Mereuta A., Pierściński K., Iakovlev V. et al. 14XX nm-wavelength electrically-pumped VECSELs fabricated by wafer fusion. Optics Express 2013; 21(11)13668.